Molecular Dipole Chains II

ARTICLE *in* THE JOURNAL OF PHYSICAL CHEMISTRY B · SEPTEMBER 1999

Impact Factor: 3.3 · DOI: 10.1021/jp991016i

2 AUTHORS:

Eunji Sim
Yonsei University
62 PUBLICATIONS **843** CITATIONS
SEE PROFILE

Mark A. Ratner
Northwestern University
905 PUBLICATIONS **42,340** CITATIONS
SEE PROFILE

Molecular Dipole Chains II

Eunji Sim* and Mark A. Ratner

Department of Chemistry, Northwestern University, Evanston, Illinois 60208

Simon W. de Leeuw

Department of Applied Physics, Delft University of Technology, 2628 CJ Delft, The Netherlands

Received: March 24, 1999; In Final Form: July 21, 1999

A simple one-dimensional dipole chain model is studied to explore the excitations and dissipation of kinetic energy in stacked planar molecular chains. At low temperatures, local dipole−dipole interaction dominates the properties of the chain. The analytic approximation agrees with molecular dynamics simulation for the low energy excitation spectrum, where acoustic mode behavior of the harmonic crystal lattice is obtained. Comparisons between antiferromagnetic and ferromagnetic dipole chains are made, and the important role of local dipole−dipole interaction is suggested. With antiferromagnetic interaction, the energy propagation occurs in three processes, while the secondary oscillation is no longer distinguishable with ferromagnetic interaction. Thermal equilibrium properties are discussed including the temperature fluctuation, dipole−dipole time correlation function, the Fourier density of correlation function, and the dispersion relation.

I. Introduction

This paper is devoted to the excitation and dissipation processes of an array of molecular dipoles, whose centers are fixed. De Leeuw et al.[1] (paper I) have investigated this for an antiferromagnetic dipole chain whose subunits rotate in the plane containing the *z*-axis (Type A, see Figure 1). This article considers the rotation around the axis linking the dipolar centers (conveniently taken as the *z*-axis) with antiferromagnetic and ferromagnetic dipole interactions; the *z*-axis projection of the dipole moment vanishes and rotational and oscillatory motions occur on the *xy*-plane (Type B, see Figure 1).

Quasi one-dimensional molecular arrays have been the object of extensive studies,[2−5] examples include ferroelectric $NaNO_2$ crystals, planar organometallic stacks and one-dimensional organic polymer chains. Special attention has been paid to the series of metallophthalocyanine polymer and stack conductors (M = H_2, Cu, Ni, and Co),[6−11] whose physical properties exhibit highly one-dimensional features at low temperatures. More recently, a number of synthetic motifs have been introduced that suggest extensive structures of controlled effective dimensionality,[12] and some interesting aspects of their energy transfer behavior have been discussed.[13]

The nonlinear dynamics of localized structures of the soliton type in lattice models has received considerable attention during the past decade.[14−19] This type of model is useful for the variety of applications including nonlinear laser excitation[20] to design a propagating coherent atomic pulse along the axis of a traveling wave laser beam. A similar model has been used to study the transport properties in hydrogen-bonded structures with dipole−dipole interactions, such as the charge and energy transfer in DNA molecules.[21−23]

We use a simple one-dimensional dipole chain model to explore particular energy transport, excitation, and dissipation of molecular stacks. A chain of essentially identical dipoles has been investigated analytically by considering nearest-neighbor interactions of the individual charges in the dipoles.[24] The true dipolar structure, however, should include long-range dipole−dipole interaction. In this manuscript, we focus on the local transport dynamics set up by an initially excited dipole, the excitation spectrum, and energy loss behavior of such an array. We treat these molecules as classical point dipoles with only long-range dipole−dipole interaction.

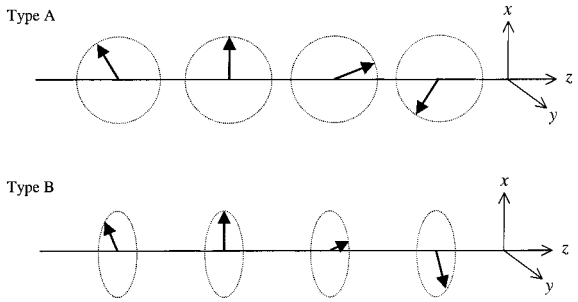

Figure 1. Schematic diagram of linear dipole chains; Type A and Type B.

In section II, the Lagrangian of the problem and the low frequency excitation spectrum are described. In section III, molecular dynamics methods are used to characterize the energy transfer from an initially excited dipole. Section IV presents the correlation and dynamics in an equilibrium system of these dipoles, and concluding remarks appear in section V.

II. Lagrangian and the Equation of Motion

The problem of linear molecular dipole array begins with the Lagrangian[1]

$$L = \frac{I}{2\mu^2}\sum_i \dot{\vec{\mu}}_i^2 + \sigma \sum_{i=1}^{N-1}\sum_{j=i+1}^{N}\left[\frac{\vec{\mu}_i\cdot\vec{\mu}_j}{r_{ij}^3} - \frac{3(\vec{\mu}_i\cdot\vec{r}_{ij})(\vec{\mu}_j\cdot\vec{r}_{ij})}{r_{ij}^5}\right] \quad (1)$$

where σ is -1 $(+1)$ for antiferromagnetic (ferromagnetic)

* Corresponding author.

10.1021/jp991016i CCC: $18.00
Published on Web 09/28/1999

coupled dipoles (physically, only the $\sigma = -1$ term is important). Here, I, $\vec{\mu}_i$, and $\vec{r}_{ij}$ are respectively the moment of intertia, the dipole moment on the ith site, and the distance vector between sites i and j.

We represent the dipole moment vector in terms of its magnitude μ and its rotational angle θ. The Lagrangian for our Type B dipole chain can be rewritten as

$$\vec{\mu}_i = \mu(\cos\theta_i, \sin\theta_i, 0) \quad \vec{r}_{ij} = r_0(0,0,j-i) \quad i = 1,\cdots,N \quad j = 1,\cdots,N$$

$$L = \frac{I}{2}\sum_i \dot{\theta}_i^2 + \sigma\frac{\mu}{r_0^3}\sum_{i=1}^{2N-1}\sum_{j=i+1}^{N}\frac{\cos(\theta_i - \theta_j)}{|j-i|^3} \tag{2}$$

where we have defined r_0 as the (constant) distance between the fixed centers of neighboring dipoles; $r_{ij} = r_0|j - i|$. Since the distance vector is perpendicular to the dipole moment vector, the second term in the double summation of eq 1 is zero. The equation of motion for the rotational angle is obtained from the Euler−Lagrange equation

$$\ddot{\theta}_i = -\sigma\omega_0^2\sum_{j\neq i}^{N}\frac{\sin(\theta_i - \theta_j)}{|j-i|^3} \tag{3}$$

with $\omega_0^2 \equiv \mu^2/Ir_0^3$. Solution of eq 3, provided by molecular dynamics simulation using the Gear 5-value predictor−corrector algorithm,[25] gives the excitation behavior of the dipole chain.

In the following subsections, we compare the low-temperature excitation spectrum and the group velocity of antiferromagnetic and ferromagnetic infinite dipole chains, with analytic approximations, and interpret the results in terms of localized and delocalized structures.

Antiferromagnetic Dipole Chain ($\sigma = -1$). Suppose we have an infinite array of dipoles. The potential energy term in eq 2 will be minimized when each dipole is antiparallel to its nearest neighbors. The ground-state potential energy corresponds to $\theta_{2i-1} = \phi =$ constant and $\theta_{2i} = \pi + \phi$, $i = 1,\cdots,N/2$ so that

$$\cos(\theta_j - \theta_i) = \begin{cases} 1 \text{ if } j-i \text{ even} \\ -1 \text{ if } j-i \text{ odd} \end{cases}$$

$$V_0 = \frac{N\mu^2}{r_0^3}\sum_{n=1}^{\infty}\frac{(-1)^n}{n^3} = -\frac{3N\mu^2}{4r_0^3}\zeta(3) = -0.9015\frac{N\mu^2}{r_0^3} \tag{4}$$

Here we have used the relation

$$\sum_{j\neq i} f(j-i) = \sum_{j=-\infty}^{i-1} f(j-i) + \sum_{j=i+1}^{\infty} f(j-i) = 2\sum_{n=1}^{\infty} f(n)$$

where the even function $f(n) = (-1)^n/|n|^3$, and the zeta function[26] is $\zeta(n) = \sum_{m=1}^{\infty} m^{-n}$. Note that the ground state is degenerate, corresponding to rotation by a constant angle around the z-axis. Therefore, the long wavelength limit of the excitation spectrum approaches zero and the rotation is a zero frequency mode.

To obtain the low energy excitation spectrum we introduce a new variable ϕ_i:

$$\theta_i = (-1)^n\frac{\pi}{2} + \phi_i \quad i = 1,\cdots,N \tag{5}$$

$$\dot{\theta}_i = \dot{\phi}_i$$

where we assumed ϕ_i to be small. The harmonic approximation of eq 3 then gives the equation of motion in the form

$$\dot{\phi}_i = \omega_0^2\sum_{j\neq i}^{N}\frac{(-1)^{j-i}}{|j-i|^3}(\phi_i - \phi_j) \tag{6}$$

The traveling wave solution with wave vector K and corresponding frequency ω_K

$$\phi_l = A_K\exp(i\omega_K t - ir_0Kl) \tag{7}$$

leads to the dispersion relation

$$\omega_K^2 + 2\omega_0^2\sum_{n=1}^{\infty}\frac{(-1)^n}{n^3}(1 - \cos(r_0Kn)) = 0 \tag{8}$$

The dispersion spectrum eq 8 is illustrated in Figure 2 where we used $\omega_0 = 1$. The frequency vanishes at $K = 0$ and reaches a maximum at $K = \pi$, resembling the acoustic mode of a harmonic lattice.[27]

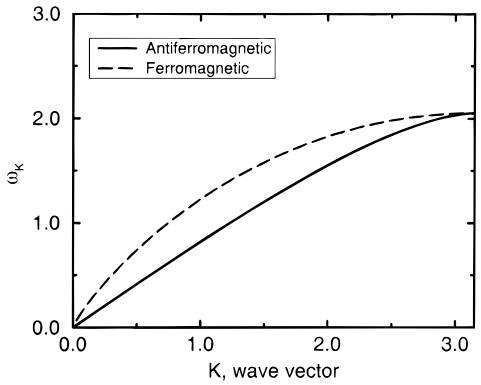

Figure 2. Dispersion curve for low energy excitations: antiferromagnetic dipole chain (eq 8) and ferromagnetic dipole chain (eq 14). Note $\omega_{K\to 0} \propto K$ and $\omega_{K=\pi} \approx 2.05$ for both chain types. Reduced units are used, $I = 1$, $\mu = 1$, and $r_0 = 1$ such that $\omega_0 = 1$.

For the long wavelength limit (i.e., $K \to 0$), eq 8 becomes

$$\omega_K^2 + r_0^2K^2\omega_0^2\sum_{n=1}^{\infty}\frac{(-1)^n}{n} = 0 \tag{9}$$

thus

$$\omega_K = \pm r_0K\omega_0\sqrt{\ln 2} = \pm 0.833r_0K\omega_0 \tag{10}$$

Alternatively, when $K = \pi$

$$\omega_{K=\pi}^2 + 2\omega_0^2\sum_{n=1}^{\infty}\frac{(-1)^n}{n^3}(1 - (-1)^n) = 0 \tag{11}$$

therefore, the dispersion spectrum attains the maximum $\omega_{K=\pi} = 2.05\ \omega_0$. From the dispersion relation, eq 8, one can also obtain the group velocity using the definition $v_g = |d\omega_K/dK|$, so that

$$v_g = \frac{-r_0}{\omega_K}\sum_{n=1}^{\infty}\frac{(-1)^n}{n^2}\sin(Kr_0n) \tag{12}$$

The group velocity in the low-temperature regime is presented in Figure 3; it maximizes at $K = 0$ with $v_g = 0.833$ (with $\omega_0 = 1$), which is approximately twice as fast as the Type A dipole chain.[1]

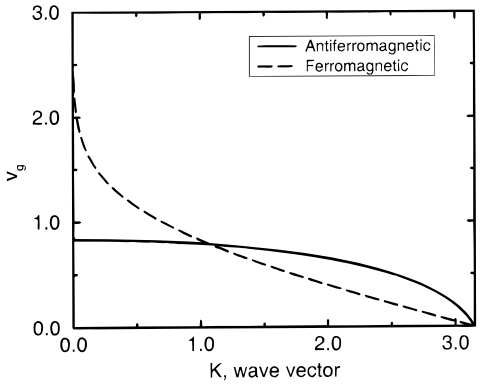

Figure 3. Group velocity, at which the excitation spreads along the chain: antiferromagnetic dipole chain (eq 12) and ferromagnetic dipole chain (eq 15). Note that the group velocity diverges as in the long wavelength limit $K \rightarrow 0$ with ferromagnetic dipole interaction. Reduced units are used, $I = 1$, $\mu = 1$, and $r_0 = 1$ such that $\omega_0 = 1$.

Ferromagnetic Dipole Chain ($\sigma = 1$). For the ferromagnetic dipole chain, the potential energy will be minimized when all of the dipoles are parallel, so that $\theta_i = \phi =$ constant, $i = 1,\cdots,N$

$$V_0 = -\frac{N\mu^2}{r_0^3}\sum_{n=1}^{\infty}\frac{1}{n^3} = -1.202\frac{N\mu^2}{r_0^3} \tag{13}$$

Again, $\omega_K \rightarrow 0$ as $K \rightarrow 0$, and the dispersion relation (Figure 2) is obtained as

$$\omega_K^2 - 2\omega_0^2\sum_{n=1}^{\infty}\frac{1}{n^3}(1 - \cos(r_0 K n)) = 0 \tag{14}$$

with the group velocity (Figure 3)

$$v_g = \frac{r_0}{\omega_K}\sum_{n=1}^{\infty}\frac{1}{n^2}\sin(r_0 K n) \tag{15}$$

Compare the dispersion spectrum and the group velocity with two different dipole interactions in Figures 2 and 3. The dispersion spectra have similar shapes, with the same values at $K \rightarrow 0$ and $K = \pi$, but saturate faster with ferromagnetic interaction. The ferromagnetic chain's group velocity diverges, eq 15, in the long wavelength limit and rapidly decreases with wave vector, while the antiferromagnetic interaction has a well-defined maximum in the limit of $K \rightarrow 0$; both vanish at $K = \pi$. The antiferromagnetic case has a linear dispersion relation over a long range in K, while the ferromagnetic case has a very short linear range.

III. Energy Transfer

To understand the nature of energy transfer processes within the molecular assembly, it is natural to characterize the decay of highly excited, initially localized kinetic energy. In the remainder of this article, we use reduced units:[1] distances are measured in units of r_0 and energies in units of $\epsilon = \mu^2/r_0^3$. The temperature is measured in ϵ/k_B, where k_B is the Boltzmann constant and the time unit is ω_0^{-1}.

Consider two linear chains of 100 dipoles: one with antiferromagnetic dipole interaction and the other with ferromagnetic dipole interaction. At initial time, all of the dipoles are resting in their equilibrium configurations and the central dipole is given a large kinetic energy. Since the chain is finite, with free end boundary conditions, one might anticipate that the transferred pulse of energy will reflect off the chain ends and return.

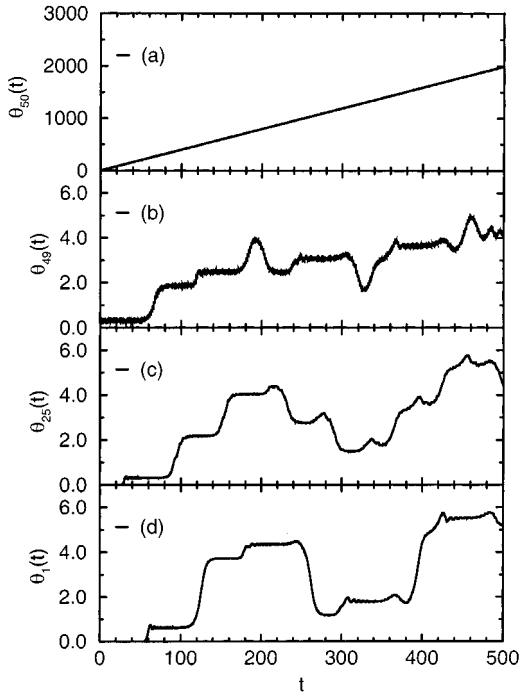

Figure 4. Time evolution of rotational angles (in radians) following the initial excitation, in a 100 unit antiferromagnetic dipole chain. The 50th dipole ((a) θ_{50}) is originally given angular velocity corresponding to a kinetic energy of 10 units. The angular position of its nearest neighbor ((b) θ_{49}) and a dipole halfway toward the end of the chain ((c) θ_{25}) and the end dipole ((d) θ_1) are shown in Figures 4b, c, and d, respectively. (Here, 0 to 2π convention is purposely not applied to show the continuous time evolution.)

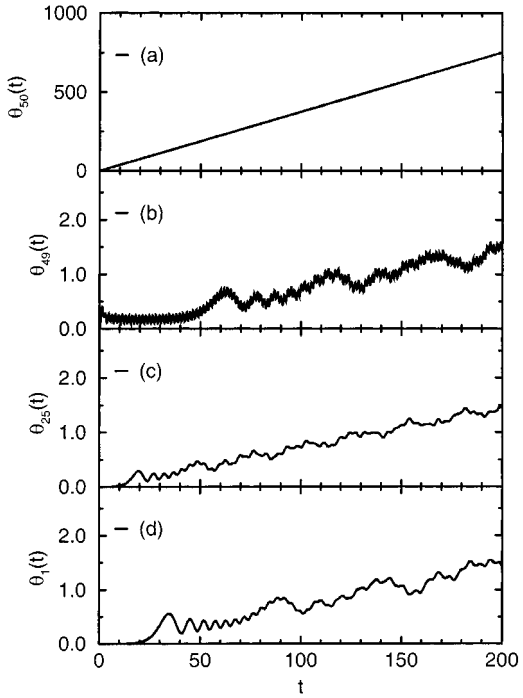

Figure 5. Time evolution of rotational angles following the initial excitation in a 100 ferromagnetic dipole chain. Positions of shown dipoles are those in Figure 4.

Figures 4 and 5 demonstrate the time evolution of the rotational angle, $\theta_i(t)$, of the chosen dipoles in the chain, following the excitation of dipole 50 (the central dipole) with

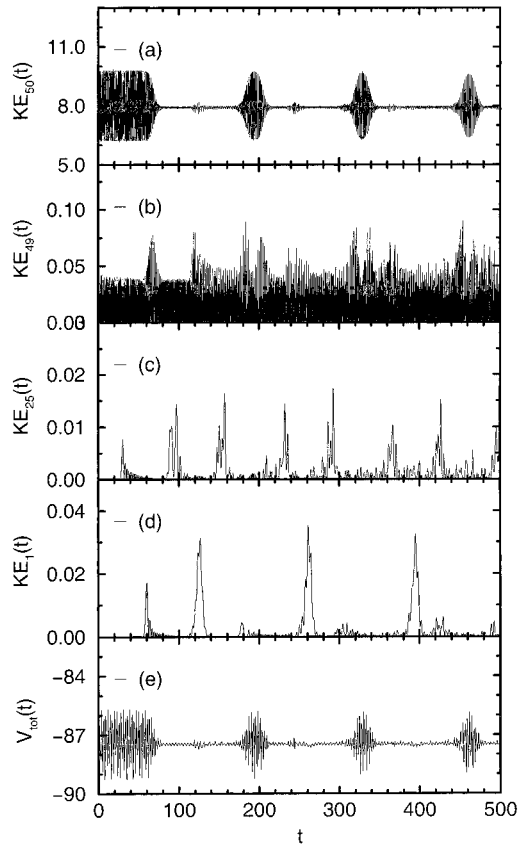

Figure 6. Time evolution of kinetic energy transfer and total potential energy of 100 unit antiferromagnetic dipole chain: (a) $KE_{50}(t)$, (b) $KE_{49}(t)$, (c) $KE_{25}(t)$, (d) $KE_1(t)$, and (e) $V_{tot}(t)$. Secondary periodic behavior is seen all of the energy profiles including the central dipole, which is initially locally excited. The major period corresponds to the returned wave front reflected at both the ends of the chain. One can easily distinguish the history of each reflected wave front by following the energy packet.

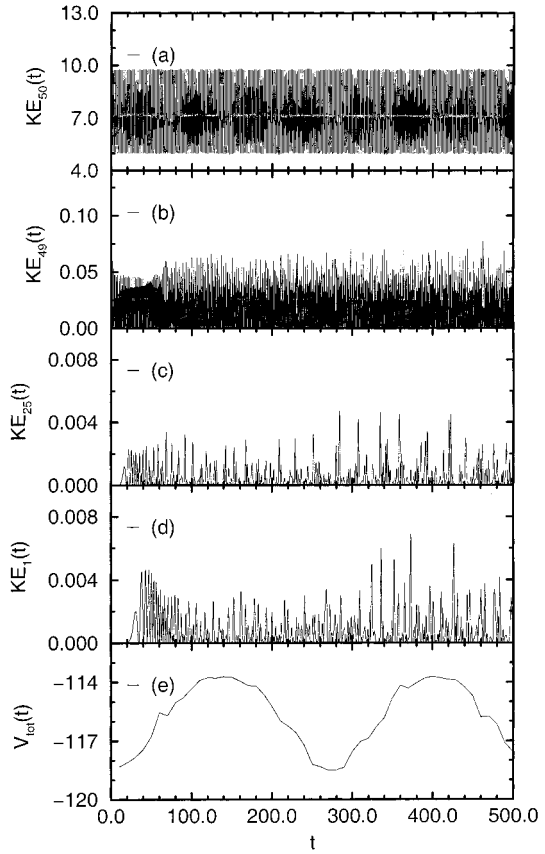

Figure 7. Time evolution of kinetic energy transfer and total potential energy of the 100 unit ferromagnetic dipole chain: (a) $KE_{50}(t)$, (b) $KE_{49}(t)$, (c) $KE_{25}(t)$, (d) $KE_1(t)$, and (e) $V_{tot}(t)$. The total potential energy profile exhibits periodic motion while no apparent secondary transfer appears in the kinetic energy profiles.

10 units of kinetic energy at time zero. Figures 4 and 5 (a−d), respectively, show the time dependence of the rotational angle of the central dipole (θ_{50}), the nearest neighbor of initially excited dipole (θ_{49}), a dipole halfway down the chain toward the end (θ_{25}), and the end dipole (θ_1). During molecular dynamics simulation up to 1000 time units, the central dipole rotates in one direction around the *z*-axis regardless of the dipole interaction type, i.e., $\theta_{50}(t) \propto t$ as in Figures 4a and 5a. The motions of other dipoles are basically local oscillations due to the dipole−dipole interaction and rotation around the *z*-axis. In the process of the energy transfer there is a distinct difference between antiferromagnetic and ferromagnetic dipole chains. With the ferromagnetic interaction in Figure 5 the rotation is rather continuous and the group velocity is faster than that of the antiferromagnetic interaction. It is striking to see, in Figure 4, discontinuous hopping-like rotation with antiferromagnetic interaction. Total angular momentum is conserved for both cases. The difference is even clearer in Figures 6 and 7, where we exhibit the time history of the total potential energy and kinetic energy for the central dipole and three chosen dipoles as shown in Figures 4 and 5. With antiferromagnetic interaction (Figure 6) the kinetic energy profile shows multiperiodic oscillations in time. The dominant period of kinetic energy packet oscillation corresponds to the returned wave front reflected at both ends of the finite chain (dipole 1 and dipole 100); this is just $100/v_g \approx 130$ time units. This periodicity is absent in the kinetic energy profile of the ferromagnetic dipole chain while total potential energy oscillates (see Figure 7).

It is intriguing to interpret the discontinuous hopping-like energy transfer in Figures 4 and 6. The energy transfer consists of three processes: instantaneous propagation with small energy intensity, the secondary oscillation that carries a substantial amount of energy, and the energy packet returned after bouncing off the ends.

(i) As soon as the central dipole rotates, some kinetic energy leaks to its nearest neighbors and the transmitted energy travels all the way to the ends of chain where the energy packet is reflected. However, the amount of kinetic energy involved is less than 0.5% of the original excitation given the central dipole.

(ii) More profound and explicit energy transfer appears after roughly 75 time units. Approximately 2 units of kinetic energy (20% of the original excitation) hops to dipoles 49 and 51 within this time in the form of kinetic and potential energy (see Figures 4b and 6b). The secondary transfer is easier to distinguish since the intensity of this kinetic energy packet is roughly twice larger than that of the initial leak (Figure 6b). By simulating different dipole chains we found only a weak correlation between the length of the chain and the initial decay lifetime of the secondary energy transfer ($\tau_{decay} \approx 68$, 75, 80 time units with 100, 150, 200 dipole chain, respectively). This suggests that the initial decay lifetime is dominated by the local dipole−dipole interaction rather than by chain length. Dipole 49 gains a maximum of 0.08 energy units from the first secondary energy transfer.

(iii) The energy packet propagates through the chain and comes back after bouncing off the ends. From Figure 6 (a−d), the period of the energy packet is estimated as approximately 128 time units, consistently, to travel 100 dipoles, such that the energy packet travels the chain with the velocity of $v_g = 100/$

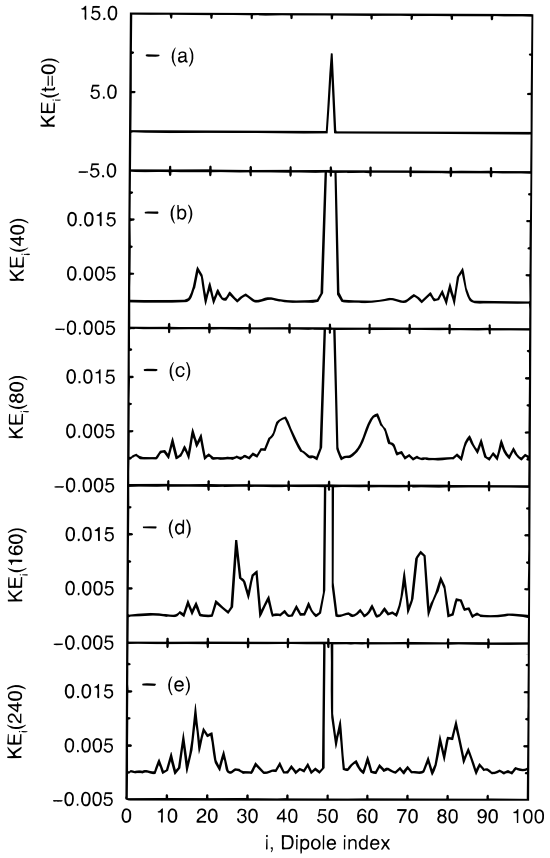

Figure 8. Snapshots of kinetic energy profile along the 100 antiferromagnetic dipole chain at chosen times: (a) $t = 0$, (b) $t = 40$, (c) $t = 80$, (d) $t = 160$, and (e) $t = 240$.

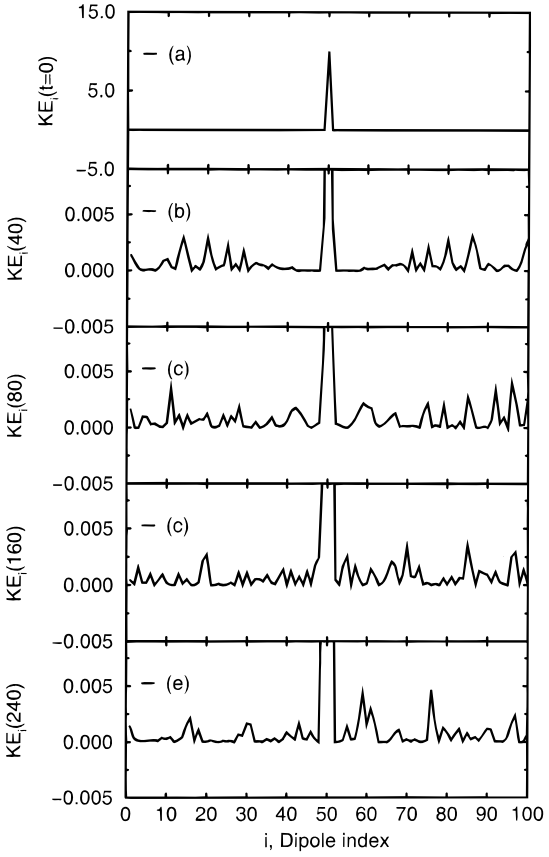

Figure 9. Snapshots of the kinetic energy profile along the 100 ferromagnetic dipole chain at chosen times: (a) $t = 0$, (b) $t = 40$, (c) $t = 80$, (d) $t = 160$, and (e) $t = 240$.

128 = 0.78. Intermediate dipoles (for example, dipole 25) receive energy from one neighbor (dipole 24/dipole 26) and deliver it to the other neighbor (dipole 26/dipole 24) coherently. The end dipole, however, obtains maximum of 0.04 units of energy because of the free end boundary condition. The end dipole has only one neighbor so that the energy accumulated before it travels back along the chain is approximately twice that at dipole 25.

With ferromagnetic interaction, it is no longer easy to distinguish the secondary transfer from the initial instantaneous leak. Even though the energy evolution is rapid, it is not favorable; the kinetic energy transferred part way down the chain (dipole 25) is roughly five times smaller than with antiferromagnetic interaction. The potential energy compensation dominates the kinetic energy transfer.

Figures 8 and 9 show snapshots of the kinetic energy profile along 100 antiferromagnetic and ferromagnetic, respectively, dipole chains at chosen times. An apparent kinetic energy packet traveling the chain is observed with antiferromagnetic chain that coincides with temporal packet shown in Figure 6; this contrasts sharply with the more mixed structure for the ferromagnetic situation.

If the molecules have a length of 25 Å and the time unit is 4 ns,[1] then the group velocity

$$v_g = \frac{0.78 \times 25 \times 10^{-10}\, M}{4 \times 10^{-9}\ \mathrm{s}} \cong 0.5\, M/\mathrm{s}$$

and the pulse period of 128 time units is $128 \times 4 \times 10^{-9}$ s = 0.5 μs.

IV. Equilibrium Dynamics and Correlation Functions

In section III, to explore the energy transfer phenomena in the molecular array, we have intentionally ignored thermal effects. In physical systems, the molecular assembly is subject to thermal forces, that will be relevant to the behavior of the molecular material. Therefore, in this section we examine dipolar correlation functions and their decays for differing temperatures and frequencies.

To simulate the equilibrium dynamics of the dipole chain, an initial kinetic energy is given to each dipole at the equilibrium configuration. The velocity is chosen randomly for large enough temperature to exceed local interactions. Relaxation will follow at that temperature until equilibrium is reached. Next, the temperature is slowly quenched until the whole chain equilibrates at the desired temperature, then the microcanonical (constant energy) sampling starts for the equilibrium dynamics and correlations. Reduced units are used for 100 dipoles, and the time step used for the integration of the equation of motion, eq 3, is 0.01 unit. Samplings for the correlation were taken in every 10 integration time steps, and the time origin has been reset after every 5 correlation samplings.

Figure 10 shows the temperature fluctuation defined by the formula

$$\delta T = \frac{\langle T^2 \rangle - \langle T \rangle^2}{\langle T \rangle} \tag{16}$$

As seen in paper I, there is a transition in behavior near $T \approx 1.3$ and $T \approx 0.9$ with antiferromagnetic and ferromagnetic dipole interaction, respectively. Below that temperature the dynamical behavior of the dipoles is largely determined by the local dipolar

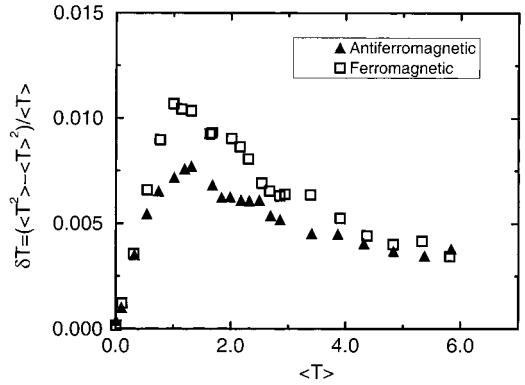

Figure 10. Temperature fluctuation as a function of temperature for the 100 dipole chains; antiferromagnetic dipoles (solid triangles) and ferromagnetic dipoles (open squares). Notice the strong peaked feature (corresponding to phase-transition-like behavior or a peak in heat capacity) near $T \approx 1.3$ (antiferromagnetic) and $T \approx 0.9$ (ferromagnetic).

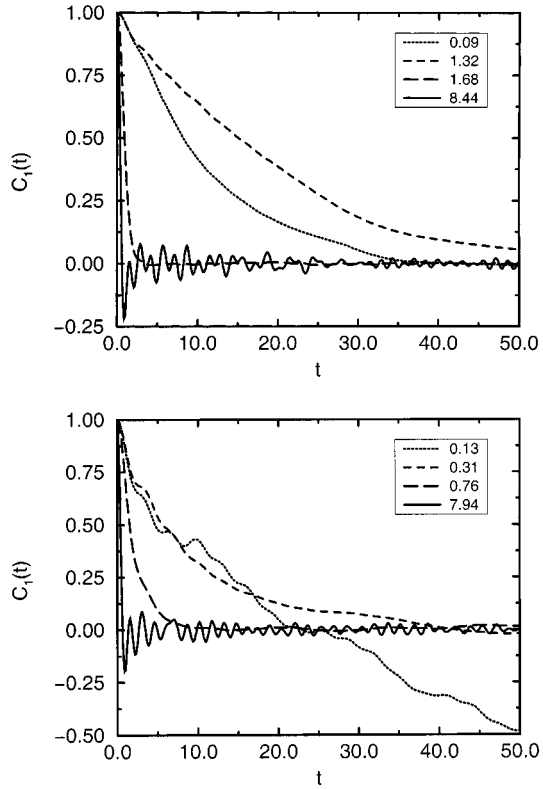

Figure 11. Dipole orientation correlation functions for the 100 dipole chains indexed by temperatures: (a) antiferromagnetic dipoles and (b) ferromagnetic dipoles. In both cases, the long-range correlations in time seen for low temperatures are substantially reduced for higher temperatures.

interactions, while for higher temperatures the thermal motion dominates the dynamics.[1]

The normalized dipole−dipole self-time correlation function is defined as

$$C_1(t) = \frac{1}{\mu^2}\langle \vec{\mu}(t)\cdot\vec{\mu}(0)\rangle \tag{17}$$

in terms of unit vectors to satisfy $C_1(0) = 1$. In Figure 11a, substantial long-range correlation at $T = 1.32$ is observed and dramatic change in the long-range correlation occurs just above this temperature, which corresponds to the peak in Figure 10. Similar long-range correlation reduction occurs at lower temperature ($T \approx 0.7$) for the ferromagnetic dipole chain in Figure 11b. Figure 11 also illustrates thermal bombardment at very high temperatures: the potential correlations are dominated by inertial effects, resulting in velocity overshoot behavior.

The correlation function of the Fourier densities, $C_2(K,t)$ is defined as

$$C_2(K,t) = C_2^0 \langle \sum_{l=1}^{N} \vec{B}_l(K,t)\cdot \sum_{m=1}^{N} \vec{B}_m^*(K,0)\rangle \tag{18}$$

where C_2^0 is the normalization constant such that $C_2(K,0) = 1$ and $K = (2\pi/N)k$, $k = 0,\cdots,N-1$. The complex vector $\vec{B}_l(K,t)$ is

$$\vec{B}_l(K,t) = (\cos(\phi_l(t))e^{ir_0Kl}, \sin(\phi_l(t))e^{ir_0Kl}) \tag{19}$$

where $\phi_l(t)$ is defined in eq 5 for antiferromagnetic and $\phi_l(t) = \theta_l(t)$ otherwise. Since $C_2(K,t)$ is real and even in time, we have used the cosine transform with a Gaussian width to obtain the Fourier component of the correlation function

$$\tilde{C}_2(K,\omega) = \frac{2}{\pi}\int_0^\tau dt\, C_2(K,t)\cos(\omega t)\exp\left[-\gamma\left(\frac{t}{\tau}\right)^2\right] \tag{20}$$

where τ is the simulation time length in molecular dynamics. The Gaussian function has been incorporated into the Fourier transform to eliminate the finite time-termination ripple. In general we have obtained reasonable quality spectra with $\gamma = 3$.

The moments of the correlation functions reflect the energy relaxation and dephasing. They are defined in the usual manner:

$$\langle \omega_K^n \rangle = \frac{\int_{-\infty}^{\infty} d\omega \omega^n \tilde{C}_2(K,\omega)}{\int_{-\infty}^{\infty} d\omega \tilde{C}_2(K,\omega)} \tag{21}$$

Since for a classical system the autocorrelation functions are even functions of time, the odd moments vanish. The second moments as a function of temperature are shown in Figure 12. At very high temperatures ($T > 7.0$), all correlations are unimportant and the even frequency moments are essentially independent of wave vector (Figure 13c). For very low temperatures, the behavior is essentially that of the dispersion relation for the acoustic phonon ($\omega_K \propto K$). In the antiferromagnetic case (Figure 12a), at intermediate temperatures $T = 1.32$, a substantial reduction in $K \rightarrow \pi$ limit of the second moment is observed; this is similar to the optical mode of harmonic crystals. Figure 13 shows the correlation function in the Fourier domain with $T = 0.09$, 1.32, and 8.44 for the antiferromagnetic dipole chain.

V. Concluding Remarks

We have calculated the excitation and dissipation of energy and thermal effects for a simple one-dimensional dipole chain that rotates around the axis linking the dipolar centers (Figure 1, Type B). At low temperatures, local dipole−dipole interaction dominates the behavior of the chain. For the low energy excitation spectrum, the approximating analytic result agrees with molecular dynamics simulation with 100 linear dipoles. The dispersion spectrum vanishes at the long wavelength limit and maximizes at $K = \pi$ regardless of the local dipole interaction type; this is essentially the behavior of the acoustic mode of a Debye crystal lattice.

The nature of energy transfer processes within the molecular assembly has been investigated following the local initial

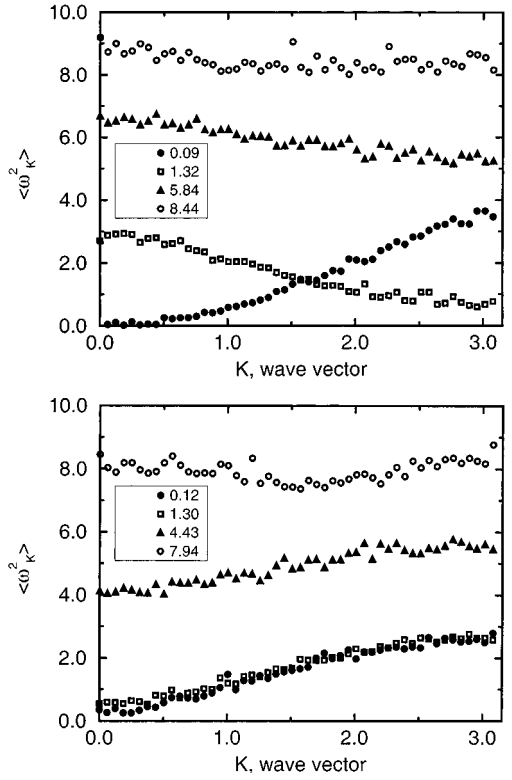

Figure 12. Temperature-dependent second moment of the correlation function indexed by temperature: (a) antiferromagnetic dipoles and (b) ferromagnetic dipoles. At very high temperatures ($T > 7.0$), all correlations are unimportant and the even frequency moments are essentially independent of wave vector. For very low temperatures, the behavior is essentially that of the dispersion relations of acoustic phonons ($\omega_K \propto K$). For the antiferromagnetic dipole chain in Figure 12a, at intermediate temperatures $T = 1.32$, a substantial reduction in the long wavelength part of the second moment is observed.

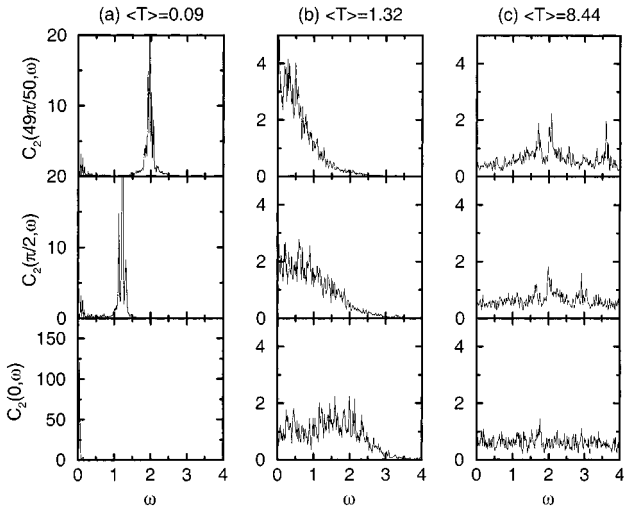

Figure 13. Fourier component of the correlation function with antiferromagnetic dipole−dipole interaction. (a) $T = 0.09$, (b) $T = 1.32$, and (c) $T = 8.44$. To show the change, the wave vectors are chosen as $K = 0$, $\pi/2$, $49\pi/50$.

excitation. The important role of local dipole−dipole interaction is suggested: with antiferromagnetic interaction, the initial energy propagation occurs in two processes, while the secondary oscillation is no longer distinguishable with ferromagnetic interaction. An initially locally excited dipole transmits minimal energy to its nearest neighbors almost instantaneously. The antiferromagnetic dipole chain develops a secondary structure for energy dissipation, which carries a substantial amount of energy. (There are some similarities between these excitations and solitons, but the obvious dissipation of these excitations is not found in solitary wave situations.) Explicit periodic motion is detected, corresponding to the returned wave front bounced at the ends of chain.

Thermal equilibrium properties have been discussed. Consistent transition behavior is seen in the temperature fluctuation, dipole−dipole time correlation function, the Fourier density of correlation function, and the dispersion relation. The dynamics is determined by local interaction at low temperatures, while for high temperatures it is the thermal bombardment that dominates the dynamics; the dynamics at high temperatures are indistinguishable between the two dipole chains. In the antiferromagnetic dipole chain at temperature $T \approx 1.3$, a substantial reduction in the $K \rightarrow \pi$ limit of the second moment is observed, similar to that in the optical mode of a harmonic lattice.

One challenging possible application of energy transfer in low-dimensional molecular assemblies is the design of switching devices that might turn on the local electric/magnetic field at the specific position of the sample, such as in a biological cell or membrane or a synthetic assembly. A two-dimensional mesh of dipoles could be carefully constructed so that a pulse of energy is sent to a specific grid point of the mesh by manipulating the phase and time of the initial signal. This microsignal may trigger processes such as primary charge transfer. Constructive and destructive interference pattern of signals can be studied with a low-dimensional array by sending the kinetic energy excitation from several different sites of the chain or mesh. The pulse structures seen in Figure 6 suggest that the antiferromagnetic chain might well support such an addressing mode.

Acknowledgment. We are grateful to the National Science Foundation for support and to Prof. Josef Michl for suggesting this problem.

References and Notes

(1) de Leeuw, S. W.; Solvaeson, D.; Ratner, M. A.; Michl, J. *J. Phys. Chem. B* **1998**, *102*, 3876.

(2) Ferraro, J. R.; Williams, J. M. *Introduction to Synthetic Electrical Conductors*; Academic: Orlando, FL, 1987. *Handbook of Conducting Polymers*; Skotheim, T., Elsenbaumer, R. L., Reynolds, J. R., Eds.; Marcel Dekker: New York, 1998.

(3) Jerome, D.; Creuzet, F.; Bourbonnais, C. *Phys. Scr. T* **1989**, *27*, 130.

(4) *Solitons and Condensed Matter Physics*; Bishop, A. R., Schneider, T., Eds.; Springer: Berlin and New York, 1981.

(5) Davydov, A. S. *Solitons in Molecular Systems*; Reidel: Dordrecht and Boston, 1985.

(6) Pietro, W.; Marks, T. J.; Ratner, M. A. *J. Am. Chem. Soc.* **1985**, *107*, 5387.

(7) Hiejima, T.; Yakushi, K. *J. Chem. Phys.* **1995**, *103*, 3950.

(8) Poirier, M.; Pouget, J. P.; Thompson, J. A.; Hoffman, B. M. *Phys. Rev. B* **1995**, *51*, 14861.

(9) Martinsen, J.; Palmer, S.; Tanaka, J.; Greene, R. R.; Hoffman, B. M. *Phys. Rev. B* **1984**, *30*, 6269.

(10) Ogawa, M. Y.; Martinsen, J.; Palmer, M. S.; Stanton, J.; Tanaka, J.; Greene, R. L.; Hoffman, B. M.; Ibers, J. A. *J. Am. Chem. Soc.* **1987**, *109*, 1115.

(11) Hale, P. D.; Ratner, M. A. *J. Chem. Phys.* **1985**, *83*, 5277. Conwell, E. M.; Mizes, H. A. *Phys. Rev. B* **1995**, *51*, 6953.

(12) *Modular Chemistry*; Michl, J., Ed.; NATO ASI Series. Series C, Mathematical and Physical Sciences 499; Kluwer Academic Publishing: Boston, 1997.

(13) Vacek, J.; Michl, J. *New J. Chem.* **1997**, *21*, 1259.

(14) Sayadi, M. K.; Pouget J. *J. Phys. A: Math. Gen.* **1991**, *24*, 2151.

(15) Rasmussen, K. O.; Christiansen P. L.; Johansson M.; Gaididei Y. B.; Mingaleev, S. F. *Physica D* **1998**, *113*, 134.

(16) Gaididei, Y. B.; Mingaleev S. F.; Christiansen P. L.; Rasmussen K. O. *Phys. Rev. E* **1997**, *55*, 6141, part B.

(17) Konotop, V. V.; Takeno S., *Phys. Rev. B: Condens. Matter* **1997**, *55*, 11342.

(18) Gaididei, Y. B.; Rasmussen K. O.; Christiansen P. L. *Phys. Lett. A* **1995**, *203*, 175.
(19) Rasmussen, K. O.; Cai D.; Bishop A. R.; GronbechJensen, N. *Phys. Rev. E* **1997**, *55*, 6151.
(20) Dyrting, S.; Zhang W. P.; Sanders B. C. *Phys. Rev. A* **1997**, *56*, 2051.
(21) Hermon, Z.; Caspi S.; Ben-Jacob E. *Europhys. Lett*. **1998**, *43*, 482.
(22) Zhang, C. T.; Chou K. C. *Chem. Phys.* **1996**, *206*, 271.
(23) Chochliouros, I.; Pouget J. *J. Phys.: Condens. Matter* **1995**, *7*, 8741.
(24) Zorski, H.; Infeld, E. *Phys. Rev. Lett.* **1992**, *68*, 1180.
(25) Allen, M. P.; Tildesley, D. J. *Computer simulation of liquids*; Oxford University Press: Oxford, 1989.
(26) See for example, Arfken, G. *Mathematical methods for physicists*, 2nd ed.; Academic Press: New York, 1970.
(27) For example, Kittel, C. *Introduction to solid-state physics*, 5th ed.; John Wiley & Sons: New York, 1976.